Floquet control of global $\mathcal{PT}$ symmetry in quadrimer waveguide arrays

Bo Zhu[1,2] Honghua Zhong,[1,3,*] Jun Jia,[4] Fuqiu Ye[4] and Libin Fu[3,†]

[1]*Institute of Mathematics and Physics, Central South University of Forestry and Technology, Changsha 410004, China*
[2]*School of Physics and Astronomy, Sun Yat-Sen University (Zhuhai Campus), Zhuhai 519082, China*
[3]*Graduate School, China Academy of Engineering Physics, Beijing 100193, China*
[4]*Department of Physics, Jishou University, Jishou 416000, China*

Manipulating the global $\mathcal{PT}$ symmetry of a non-Hermitian composite system is a rather significative and challenging task. Here, we investigate Floquet control of global $\mathcal{PT}$ symmetry in quadrimer waveguide arrays with transverse periodic structure along the x axis and longitudinal periodic modulation along the z axis. For the unmodulated case with inhomogeneous inter- and intraquadrimer coupling strength $\kappa_1 \neq \kappa$, in addition to the conventional global $\mathcal{PT}$ symmetric phase and the $\mathcal{PT}$ symmetry breaking phase, we find that there is an exotic phase in which global $\mathcal{PT}$ symmetry is broken under open boundary condition, whereas it still is unbroken under periodical boundary condition. Especially, the domain of the exotic phase induced by boundary effect can shrink and even disappear by tuning modulation parameter. More interestingly, whether or not the array has initial global $\mathcal{PT}$ symmetry, periodic modulation can not only restore the broken global $\mathcal{PT}$ symmetry, but also control it by tuning modulation amplitude. Therefore, the global property of transverse periodic structure of such an array can be manipulated by only tuning modulation amplitude of longitudinal periodic modulation.

I. INTRODUCTION

Global parity-time ($\mathcal{PT}$) symmetry plays a key role in determining the real energy spectrum, topological character, and transport property of non-Hermitian composite systems [1–8]. There are many interesting physical phenomena related to global $\mathcal{PT}$ symmetry, including topological bound state [9], edge-mode lasing [10], anomalous edge states [11], and anisotropic transmission resonances [12]. A characteristic property of global $\mathcal{PT}$ symmetric system is the existence of a phase transition (spontaneous global $\mathcal{PT}$ symmetry breaking) from the unbroken to broken $\mathcal{PT}$ symmetric phase whenever the gain or loss parameter exceeds a certain threshold. This has been experimentally demonstrated in synthetic photonic lattices [9,13] and cavity laser arrays [14]. Therefore, an important issue in a global $\mathcal{PT}$ symmetric system is the ability to control and tune this phase transition.

Optical structures constructed by arrays of coupled dimers [15–23], trimer [24], or quadrimers [25–27] provide a fertile ground to observe and utilize notions of global $\mathcal{PT}$ symmetry. Global $\mathcal{PT}$ symmetry of such system will require precise relation between various on-site energies and coupling symmetry in the building blocks, and hence becomes extremely fragile in the presence of disorder, impurities, and boundaries which can support localized modes [28–33]. One of the most significant features of such optical structures is the boundary condition dependence, where systems under periodic boundary condition (PBC) and open boundary condition (OBC) have dramatically different energy spectra, and the zero-energy edge states (topologically nontrivial phase) re-

lated to spontaneous global $\mathcal{PT}$ symmetry breaking transition can appear under open boundary condition. These have received great research interests in a class of photonic arrays of $\mathcal{PT}$ symmetric dimers described by the non-Hermitian Su-Schrieffer-Heeger (SSH) model [34–39]. It was shown that there is no universal correlation between spontaneously global $\mathcal{PT}$ symmetry breaking and the topologically nontrivial phase, and only the symmetry of the individual edge states can decide whether their presence has an influence on the global $\mathcal{PT}$ symmetry [35]. Boundary effects on $\mathcal{PT}$ symmetry breaking and stability have been recently presented in Refs. [40] and [41] using a tight-binding dimer lattice model with only a pair of $\mathcal{PT}$ symmetric waveguides or periodically placed gain and loss element. In such works, it was suggested that $\mathcal{PT}$ symmetry breaking thresholds are different for planar and circular arrays [40]. However, such previous studies have been limited to consider static (i.e., unmodulated) arrays, and the way to manipulate the effect of the boundary influencing $\mathcal{PT}$ symmetry is still unclear.

Recently, based on the high-frequency Floquet method to rescale the coupling strength, periodic modulations have been proposed to control $\mathcal{PT}$ symmetry of single optical dimer [42–49]. It has been found that manipulation of the $\mathcal{PT}$-phase transition can be achieved by adjusting modulation parameter. The Floquet $\mathcal{PT}$ symmetric system also has been realized for two coupled LC resonators with balanced gain and loss [50]. However, these previous works mainly consider that out-of-phase periodic modulations were introduced on complex on-site energies or intradimer coupling strength. This is a rather challenging task in optical experiment, as the balanced gain and loss and periodic modulation in the complex refractive index must be tuned simultaneously. Therefore, the protocol that the additional modulated dimer is introduced to constitute a periodically modulated $\mathcal{PT}$ symmetric quadrimer

*hhzhong115@163.com
†lbfu@gscaep.ac.cn

may be more easily operated in experiment. Especially, the study on Floquet control of global $\mathcal{PT}$ symmetry in such a composite array is still lacking.

In this work, we address above these important questions by investigating global $\mathcal{PT}$ symmetry and its Floquet control in quadrimer waveguide arrays with transverse periodic structure along the x axis and longitudinal periodic modulation along the z axis, whose single quadrimer is coupled by a $\mathcal{PT}$ symmetric dimer and a periodically modulated dimer. We find that there exists an exotic phase where global $\mathcal{PT}$ symmetry is broken under OBC, whereas it still is unbroken under PBC, which may lead to the appearance of a triple point, and different broken ways of global $\mathcal{PT}$ symmetry. By comparing on the energy spectra and dynamics in the different phases, it is revealed that there exists a pair of zero-energy edge states with purely imaginary energy eigenvalues localized at the left boundary in such an exotic phase, whereas other eigenvalues are real. Especially, the domain of the exotic phase induced by boundary effect can be manipulated to be narrow and even disappears by tuning modulation parameter A/ω. More interestingly, regardless of the initial global $\mathcal{PT}$ symmetry, periodic modulation can not only restore the broken global $\mathcal{PT}$ symmetry, but also control it by tuning modulation amplitude. Therefore, the global property of such transverse periodic structure can be manipulated by only tuning modulation amplitude of longitudinal periodic modulation, which provides a promising approach for designing and manipulating optical material and may have specific technological importance.

The rest of the paper is organized as follows. In Sec. II, we give a physical description of the model. In Sec. III, we discuss the effect of the boundary on the global $\mathcal{PT}$ symmetry. In this section, we show the phase diagram for the system in the different boundary conditions and parameters in the first subsection and then discuss the energy spectra and dynamics in the different phases in the second subsection. In Sec. IV, we discuss the effect of the periodic modulation on the global $\mathcal{PT}$ symmetry and boundary effect in the high-frequency limit. At last, we give a conclusion in Sec. V.

II. MODEL

We consider an array comprised by N quadrimer waveguides, whose single quadrimer is coupled by a $\mathcal{PT}$-metric dimer and a periodically modulated dimer; see Fig. 1. Within a tight-binding model with nearest-neighbor couplings, light dynamics in the optical structure along the propagation axis z are described by the following coupled-mode equation:

$$i\frac{\partial \psi(z)}{\partial z} = H_N(z)\psi(z), \quad (1)$$

with the Hamiltonian

$$H_N(z) = \begin{pmatrix} h_1 & \sigma_+ & 0 & \cdots & 0 & 0 & 0 \\ \sigma_- & h_2 & \sigma_+ & 0 & \cdots & 0 & 0 \\ 0 & \sigma_- & h_3 & \sigma_+ & 0 & \cdots & 0 \\ \vdots & \ddots & \ddots & \ddots & \ddots & \ddots & \vdots \\ 0 & \cdots & 0 & \sigma_- & h_{N-2} & \sigma_+ & 0 \\ 0 & 0 & \cdots & 0 & \sigma_- & h_{N-1} & \sigma_+ \\ 0 & 0 & 0 & \cdots & 0 & \sigma_- & h_N \end{pmatrix}, \quad (2)$$
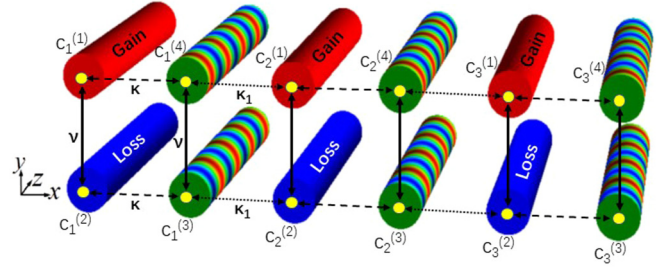

FIG. 1. Schematic diagram of a waveguide array comprised by periodically modulated $\mathcal{PT}$ symmetric quadrimers. The periodic change of color along the z axis denotes the periodic modulation $A\sin(\omega z)$. The intradimer coupling strength ν is tuned by adjusting the center-to-center waveguide spacing along the y axis, Δy; the intraquadrimer coupling strength κ and the interquadrimer coupling strength κ_1 are tuned by intermittently adjusting the center-to-center waveguide spacing along the x axis, Δx.

where

$$h_n = \begin{pmatrix} i\gamma & \nu & 0 & \kappa \\ \nu & -i\gamma & \kappa & 0 \\ 0 & \kappa & -A\sin(\omega z) & \nu \\ \kappa & 0 & \nu & A\sin(\omega z) \end{pmatrix}, \quad (3)$$

$$\sigma_- = \begin{pmatrix} 0 & 0 & 0 & \kappa_1 \\ 0 & 0 & \kappa_1 & 0 \\ 0 & 0 & 0 & 0 \\ 0 & 0 & 0 & 0 \end{pmatrix}, \quad \sigma_+ = \begin{pmatrix} 0 & 0 & 0 & 0 \\ 0 & 0 & 0 & 0 \\ 0 & \kappa_1 & 0 & 0 \\ \kappa_1 & 0 & 0 & 0 \end{pmatrix}.$$

Here $\psi(z) = [\psi_1(z), \psi_2(z), \psi_3(z), \ldots, \psi_N(z)]^T$ with $\psi_n(z) = [c_n^{(1)}(z), c_n^{(2)}(z), c_n^{(3)}(z), c_n^{(4)}(z)]^T$, and $c_n^{(j)}(z)$ is the complex field amplitude in the jth waveguide of nth quadrimer for $j = 1, 2, 3, 4$ and $n = 1, 2, 3, \ldots, N$. The diagonal blocks h_n describe the Hamiltonian of nth isolated quadrimer, and the off-diagonal block matrix $\sigma_\pm$ describes the coupling between two nearest quadrimers, where γ is the gain or loss parameter, A is the modulation amplitude, and ω is the modulation frequency. The intradimer coupling strength is ν, which can be tuned by adjusting the distance between the waveguides along the y axis, Δy. The intraquadrimer coupling strength κ and the interquadrimer coupling strength κ_1 can be tuned by intermittently adjusting the distance between the waveguides along the x axis, Δx [51]. Our system has the transverse periodic structure along the x axis with respect to N. When N is finite [$\psi_0(z) = 0$ and $\psi_{N+1}(z) = 0$], the system is analyzed under open boundary condition. When $N \rightarrow \infty$ [$\psi_0(z) = \psi_N(z)$ and $\psi_{N+1}(z) = \psi_1(z)$], the system is analyzed under periodic boundary condition. Without loss of generality, we choose $\nu = 1$ to set the energy scale and set all the parameters in units of ν throughout this paper.

Under PBC, by implementing a Fourier transform

$$c_n^{(1)} = \frac{1}{\sqrt{N}} \sum_q e^{iq(4n-3)} c_{1,q},$$

$$c_n^{(2)} = \frac{1}{\sqrt{N}} \sum_q e^{iq(4n-2)} c_{2,q},$$

$$c_n^{(3)} = \frac{1}{\sqrt{N}} \sum_q e^{iq(4n-1)} c_{3,q},$$

$$c_n^{(4)} = \frac{1}{\sqrt{N}} \sum_q e^{iq(4n)} c_{4,q},$$

one can obtain the Hamiltonian in momentum space

$$H(q,z) = \begin{bmatrix} i\gamma & v\,e^{iq} & 0 & \kappa_a \\ v\,e^{-iq} & -i\gamma & \kappa_b^* & 0 \\ 0 & \kappa_b & -A\sin(\omega z) & v\,e^{iq} \\ \kappa_a^* & 0 & v\,e^{-iq} & A\sin(\omega z) \end{bmatrix}, \tag{4}$$

where $\kappa_a = \kappa\,e^{i3q} + \kappa_1 e^{-iq}$, $\kappa_b = \kappa\,e^{-iq} + \kappa_1 e^{i3q}$, and q denotes quasimomentum. Obviously, our system has two types of periodic characters, the transverse periodic structure along the x axis and the longitudinal periodic modulation along the z axis [52]. Meanwhile, its Hamiltonian is characterized by two types of $\mathcal{PT}$ symmetries, the local and global ones. We say that the system is locally $\mathcal{PT}$ symmetric if the isolated quadrimer is $\mathcal{PT}$ symmetric in the limit $\kappa_1 = 0$. Obviously, the Hamiltonian $H_1(z)$ is $\mathcal{PT}$ symmetric due to $[H_1(z), \mathbb{P}\mathbb{T}] = 0$, where $\mathbb{P}$ is a space-reversal linear operator

$$\mathbb{P} = \begin{pmatrix} 0 & 1 & 0 & 0 \\ 1 & 0 & 0 & 0 \\ 0 & 0 & 0 & 1 \\ 0 & 0 & 1 & 0 \end{pmatrix},$$

and time operator $\mathbb{T}$ reverses the propagation direction: $\mathbb{T}$: $i \to -i$, $z \to -z$. On the other hand, we say that the system is globally $\mathcal{PT}$ symmetric if the infinite array (1) with the matrix $H(q,z)$ in (4) is $\mathcal{PT}$ symmetric for $\kappa_1 \neq 0$ [8,26]. The array in Fig. 1 consists of quadrimers which have unbroken local $\mathcal{PT}$ symmetry, at least for small γ.

III. BOUNDARY INDUCED GLOBAL $\mathcal{PT}$ SYMMETRY BREAKING

In this section, we show how the boundary, system size, and interquadrimer coupling affect the global $\mathcal{PT}$ symmetry of the system. In subsection A, we show how to obtain the phase diagram via analyzing the eigenvalues of the system under PBC and OBC. In subsection B, we show the energy spectra and dynamics in the three typical phases: robust global $\mathcal{PT}$ symmetry (R-$\mathcal{PT}$), boundary influencing global $\mathcal{PT}$ symmetry (BI-$\mathcal{PT}$), and broken global $\mathcal{PT}$ symmetry (B-$\mathcal{PT}$) phases.

A. Phase diagram

We use the usual unmodulated system as a reference system. For $A = 0$, the four eigenvalues of Eq. (4) are given by

$$E = \pm\sqrt{D + v^2 - \frac{\gamma^2}{2} \pm \frac{1}{2}\sqrt{4D(4v^2 - \gamma^2) + \gamma^4}}, \tag{5}$$

with $D = \kappa^2 + \kappa_1^2 + 2\kappa\kappa_1 \cos(4q)$ and $q \in [-\frac{\pi}{4}, \frac{\pi}{4}]$. For a fixed q, the $\mathcal{PT}$ symmetry breaking transition point is deter-
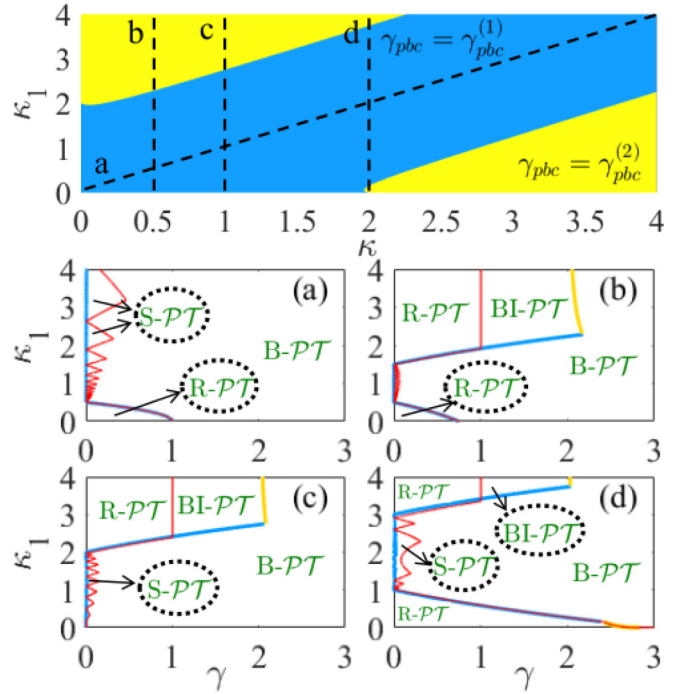

FIG. 2. (Top) Selection of the conditions $\gamma_{\text{pbc}}^{(1)}$ and $\gamma_{\text{pbc}}^{(2)}$ in the parameter plane (κ, κ_1). (a)–(d) Phase diagram for the system in the parameter plane (γ, κ_1) for (a) $\kappa = \kappa_1$, (b) $\kappa = 0.5$, (c) $\kappa = 1$, and (d) $\kappa = 2$. Light blue and yellow lines are analytical results obtained by the formula (6) under PBC and red lines are numerical results obtained from the Hamiltonian (2) under OBC. The other parameters are chosen as $N = 20$, $A = 0$, and $v = 1$.

mined by the minimum value of $|\gamma'(q)|$, where $\gamma'(q)$ satisfy

$$\gamma'(q) = \begin{cases} \pm(D - v^2)/v \\ \pm\sqrt{2D - 2\sqrt{D^2 - 4Dv^2}}. \end{cases} \tag{6}$$

Because all eigenvalues in Eq. (5) must be real for all quasimomentum q in global $\mathcal{PT}$ symmetric region, the critical value γ_{pbc} of global $\mathcal{PT}$ symmetry breaking transition is determined by the minimum value of the set $\{|\gamma'(-\frac{\pi}{4})|, \ldots, |\gamma'(\frac{\pi}{4})|\}$. For simplicity, we only consider $\gamma > 0$, and label $\gamma_{\text{pbc}}^{(1)} = \min[|(D - v^2)/v|]$ and $\gamma_{\text{pbc}}^{(2)} = \min[|\sqrt{2D - 2\sqrt{D^2 - 4Dv^2}}|]$. Then, the global $\mathcal{PT}$ symmetry is unbroken when γ satisfy

$$0 < \gamma \leqslant \gamma_{\text{pbc}}, \tag{7}$$

where $\gamma_{\text{pbc}} = \min[\gamma_{\text{pbc}}^{(1)}, \gamma_{\text{pbc}}^{(2)}]$. By comparing the magnitude of $\gamma_{\text{pbc}}^{(1)}$ and $\gamma_{\text{pbc}}^{(2)}$, the selection of the conditions $\gamma_{\text{pbc}}^{(1)}$ and $\gamma_{\text{pbc}}^{(2)}$ in the parameter plane (κ, κ_1) is given in Fig. 2 (top). Then, by changing the parameters (κ, κ_1) along the four black dashed lines (a)–(d) in Fig. 2 (top), we show the phase diagram of global $\mathcal{PT}$ symmetry in the parameter plane (γ, κ_1) in Figs. 2(a)–2(d), respectively. Obviously, depending on values of κ_1 and γ, the whole parameter space is divided into four phases: (i) robust global $\mathcal{PT}$ symmetry (R-$\mathcal{PT}$) phase, where global $\mathcal{PT}$ symmetries are unbroken both under PBC and OBC; (ii) boundary influencing global $\mathcal{PT}$ symmetry (BI-$\mathcal{PT}$) phase, where global $\mathcal{PT}$ symmetry is broken under

OBC, whereas it still is unbroken under PBC; (iii) system size affecting global $\mathcal{PT}$ symmetry (S-$\mathcal{PT}$) phase, where global $\mathcal{PT}$ symmetry is unbroken under OBC, whereas it is broken under PBC; (iv) broken global $\mathcal{PT}$ symmetry (B-$\mathcal{PT}$) phase, where global $\mathcal{PT}$ symmetries are broken both under PBC and OBC. For the homogeneous coupling case of $\kappa_1 = \kappa$, because there is no boundary effect, there does not exist BI-$\mathcal{PT}$ phase. In addition, because the limited values of $\gamma_{pbc}^{(1)}$ and $\gamma_{pbc}^{(2)}$ always approach zero with the increase of κ_1 for $\kappa = \kappa_1$, the global $\mathcal{PT}$ symmetry always is destroyed by increasing κ_1, as shown in Fig. 2(a). For the inhomogeneous coupling case of $\kappa \neq \kappa_1$, the phase space (γ, κ_1) can be divided into multiple domains consisting of R-$\mathcal{PT}$, BI-$\mathcal{PT}$, S-$\mathcal{PT}$, and B-$\mathcal{PT}$, as shown in Figs. 2(b)–2(d). An important feature of the phase diagram is the existence of the triple point that corresponds to values where three phases of R-$\mathcal{PT}$, BI-$\mathcal{PT}$, and B-$\mathcal{PT}$ touch. Thus, depending on how parameters γ and κ_1 change in vicinity of the triple point, breaking of global $\mathcal{PT}$ symmetry can occur in two different ways: R-$\mathcal{PT} \rightarrow$ B-$\mathcal{PT}$ or R-$\mathcal{PT} \rightarrow$ BI-$\mathcal{PT} \rightarrow$ B-$\mathcal{PT}$.

As shown in Ref. [29], our unmodulated system under OBC can support a pair of degenerate eigenstates that are the symmetric and antisymmetric superpositions of two well-localized states centered symmetrically near the left boundary of the system, and these pairs form effective dimer, exactly as the single $\mathcal{PT}$ symmetric dimer. Therefore, the maximal critical value of global $\mathcal{PT}$ symmetry breaking transition under OBC is $\widetilde{\gamma}_{obc} = \nu = 1$. Then, the critical value of global $\mathcal{PT}$ symmetry breaking transition under OBC only can be restored to $\gamma_{obc} = \widetilde{\gamma}_{obc} = 1$ by increasing κ_1. When $\widetilde{\gamma}_{obc} < \gamma < \gamma_{pbc}$, this implies that global $\mathcal{PT}$ symmetry of the system under OBC is broken, whereas it still is unbroken under PBC for certain parameter κ_1, and hence the boundary can induce global $\mathcal{PT}$ symmetry breaking. The phenomenon that boundaries can induce different $\mathcal{PT}$ symmetry breaking thresholds for planar and circular arrays composing a pair of $\mathcal{PT}$ symmetric waveguides also has been presented [40]. Here, we mainly focus on the explanation of the physical origin of the occurring BI-$\mathcal{PT}$ phase and how to manipulate it.

B. Energy spectra and dynamics in the different phases

To get deeper physical insights into the properties and the mechanism underlying the formation of BI-$\mathcal{PT}$ phase, we will show the spectra change in different phases with the increase of γ for the system under PBC and OBC. A typical example is displayed in Fig. 3 by choosing $\kappa = 0.5$, $\kappa_1 = 2.5$, and $\nu = 1$, which can undergo two phase transitions from R-$\mathcal{PT}$ phase to BI-$\mathcal{PT}$ phase and from BI-$\mathcal{PT}$ phase to B-$\mathcal{PT}$ phase as γ continuously increase. It is clear that in the R-$\mathcal{PT}$ phase the system has a purely real spectrum when $\gamma < 1$ both under PBC and OBC. However, a careful comparison of the eigenvalues reveals that a pair of isolated edge states with real spectrum begin to emerge in the middle of the energy gap under OBC. After undergoing a phase transition from R-$\mathcal{PT}$ phase to BI-$\mathcal{PT}$ phase at $\gamma = 1$, the real parts of the eigenvalues of this pair of edge states become twofold degenerate zero-energy levels; meanwhile, their imaginary parts split into one pair of nonzero conjugated imaginary values. Therefore, in the BI-$\mathcal{PT}$ phase, there exists a pair of isolated zero-energy
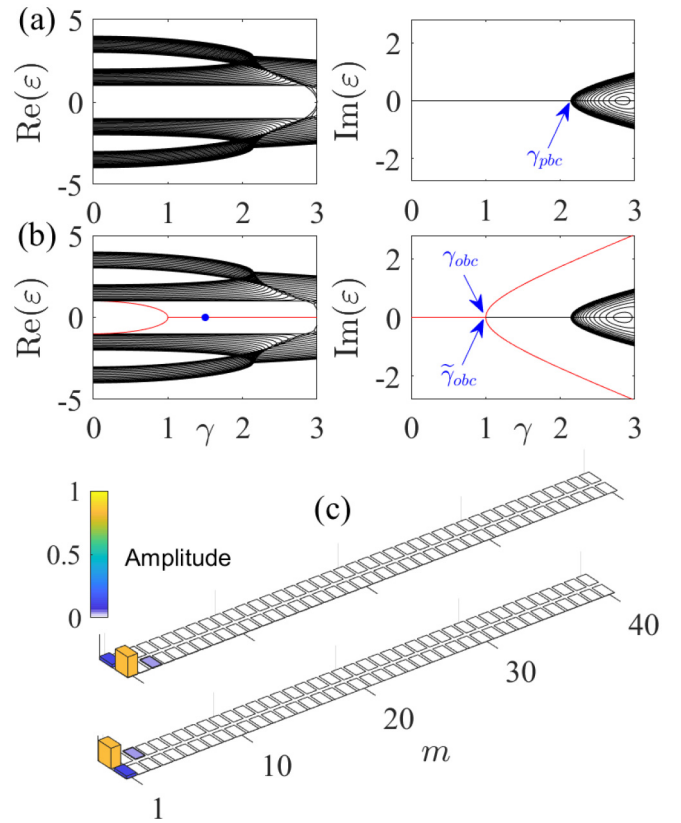

FIG. 3. (a), (b) Real and imaginary parts of the eigenvalues as a function of γ for system under PBC (top) and OBC (bottom). (c) Representative eigenstates of zero energy at $\gamma = 1.5$ [blue dot in (b)]. The other parameters are $A = 0$, $\kappa_1 = 2.5$, $\kappa = 0.5$, $N = 20$, and $\nu = 1$.

edge states with purely imaginary energy eigenvalues localized at the left boundary, whereas other $4N - 2$ eigenvalues of bulk states are real; see Fig. 3(b). Therefore, the essence of the first phase transition from R-$\mathcal{PT}$ phase to BI-$\mathcal{PT}$ phase is the transition of a pair of edge states of the system from real eigenvalues to complex eigenvalues, and the critical value is $\gamma = \widetilde{\gamma}_{obc} = 1$. This is why the boundary can break global $\mathcal{PT}$ symmetry in our system. Of course, a pair of isolated edge states with purely real eigenvalues localized at the right boundary also can occur with the increase of κ_1, but they are not zero energy. After undergoing second phase transition from BI-$\mathcal{PT}$ phase to B-$\mathcal{PT}$ phase at $\gamma = \gamma_{pbc}^{(2)}$, the real parts of $4N - 2$ ($4N$ under PBC) eigenvalues of bulk states begin to be degenerate; meanwhile, their imaginary parts begin to split into many pairs of nonzero conjugated imaginary values. Therefore, the essence of the second phase transition from BI-$\mathcal{PT}$ phase to B-$\mathcal{PT}$ phase is the transition of bulk states of the system from real eigenvalues to complex eigenvalues.

Through numerical integration, we analyze the light propagations of the coupled-mode system (1) in three different phases with $N = 20$. The light propagation sensitively depends upon the eigenvalues. Stationary light propagations of bounded intensity oscillations appear if all eigenvalues are real. Local light propagations of unbounded intensity oscillations appear if at least one of the eigenvalues is complex. To do this, we first define the light intensities in top row waveguides
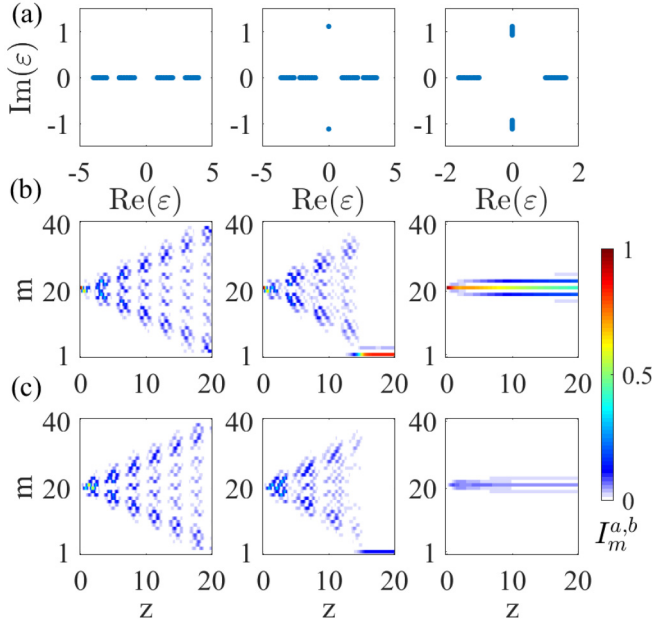
FIG. 4. (Upper) Eigenvalue distribution in the complex-energy plane. The wave-packet evolution in top [(b) panels] and bottom [(c) panels] row waveguides, respectively. In the left column we choose parameters in R-$\mathcal{PT}$ phase, such as $\kappa = 0.5$, $\kappa_1 = 2.5$, and $\gamma = 0.5$. In the middle column we choose parameters in BI-$\mathcal{PT}$ phase, such as $\kappa = 0.5$, $\kappa_1 = 2.5$, and $\gamma = 1.5$. In the right column we choose parameters in B-$\mathcal{PT}$ phase, such as $\kappa = 0.5$, $\kappa_1 = 0.5$, and $\gamma = 1.5$. The other parameters are chosen as $N = 20$ and $\nu = 1$.

$I^a_{2n-s(j)} = |c^j_n(z)|^2$ for $n = 1, 2, 3, \ldots, N$ and $j = 1$, and 4, where $s(1) = 1$ and $s(4) = 0$. Similarly, the light intensities in bottom row waveguides are defined as $I^b_{2n-s(j)} = |c^j_n(z)|^2$ for $j = 2$, and 3, where $s(2) = 1$ and $s(3) = 0$. In Fig. 4, we give the relative intensity distribution using single-site excitation away from the edge waveguide. If we choose parameters in R-$\mathcal{PT}$ phase, the light always diffracts irrespective of its input cell; see the left column in Fig. 4. If we choose parameters in BI-$\mathcal{PT}$ phase, local light propagating along the edge route appears at the left edge of the system; see the middle column in Fig. 4. The local light propagating along the left edge route is a direct signature of the BI-$\mathcal{PT}$ phase. This implies that our system can be used to realize single edge-mode lasing or robust one-way edge mode transport [10]. If we choose parameters in B-$\mathcal{PT}$ phase, the light propagating always localizes at its input cell, and propagates with unbounded intensity oscillations; see the right column in Fig. 4. Therefore, our numerical simulations of the coupled-mode system (1) perfectly confirm the BI-$\mathcal{PT}$ phase predicted by our analytical results.

IV. MANIPULATION OF GLOBAL $\mathcal{PT}$ SYMMETRY

In this section, we will explore how to manipulate the global $\mathcal{PT}$ symmetry via the periodic modulation. According to the Floquet theorem, similar to the Bloch states, the Floquet states of the modulated system (1) $\{\psi_1(z), \psi_2(z), \psi_3(z), \ldots, \psi_n(z)\} = e^{-i\epsilon z}\{\widetilde{\psi}_1(z), \widetilde{\psi}_2(z), \widetilde{\psi}_3(z), \ldots, \widetilde{\psi}_n(z)\}$. Here, the propagation constant ϵ is called the quasienergy, and the complex amplitudes

$\widetilde{\psi}_n(z + T) = \widetilde{\psi}_n(z)$ are periodic with the modulation period $T = 2\pi/\omega$. Then the quasienergies and eigenfunctions are given by $\mathcal{F}\widetilde{\psi}_n(z) = \epsilon\widetilde{\psi}_n(z)$, with the Floquet operator $\mathcal{F} = -i\frac{d}{dz} + H_N(z)$. In general, for arbitrary modulation frequency, the quasienergies and their eigenfunctions can be numerically calculated from the original Hamiltonian (2) by diagonalizing the one-periodic evolution operator $\hat{U}_T = \hat{\tau}\,e^{-i\int_0^T H_N(z)dz}$ with $\hat{\tau}$ executing the time ordering [53], where $\hat{U}_T$ satisfies $\hat{U}_T\widetilde{\psi}_n(0) = e^{-i\epsilon T}\widetilde{\psi}_n(0)$. Because in the high-frequency regime, the high-frequency terms can be averaged and the modulated system can be described by an effectively nonmodulated one with rescaled parameters [46], the high-frequency case is considered in the following.

Under the condition of $(\kappa, \kappa_1) \ll \max[\omega, \sqrt{|A|\omega}]$, one can implement the high-frequency Floquet analysis. Under OBC, by introducing the following transformation

$$c^{(1)}_n = \bar{c}^{(1)}_n,$$
$$c^{(2)}_n = \bar{c}^{(2)}_n,$$
$$c^{(3)}_n = \bar{c}^{(3)}_n e^{-i\frac{A}{\omega}\cos(\omega z)},$$
$$c^{(4)}_n = \bar{c}^{(4)}_n e^{i\frac{A}{\omega}\cos(\omega z)},$$

and averaging the high-frequency terms, one can obtain an effectively unmodulated system $i\frac{\partial \bar{c}^{(j)}_n}{\partial z} = H^{\text{eff}}_N \bar{c}^{(j)}_n$. The effective Hamiltonian can be written as

$$H^{\text{eff}}_N = \begin{pmatrix} \widetilde{h}_1 & \widetilde{\sigma}_+ & 0 & \cdots & 0 & 0 & 0 \\ \widetilde{\sigma}_- & \widetilde{h}_2 & \widetilde{\sigma}_+ & 0 & \cdots & 0 & 0 \\ 0 & \widetilde{\sigma}_- & \widetilde{h}_3 & \widetilde{\sigma}_+ & 0 & \cdots & 0 \\ \vdots & \ddots & \ddots & \ddots & \ddots & \ddots & \vdots \\ 0 & \cdots & 0 & \widetilde{\sigma}_- & \widetilde{h}_{N-2} & \widetilde{\sigma}_+ & 0 \\ 0 & 0 & \cdots & 0 & \widetilde{\sigma}_- & \widetilde{h}_{N-1} & \widetilde{\sigma}_+ \\ 0 & 0 & 0 & \cdots & 0 & \widetilde{\sigma}_- & \widetilde{h}_N \end{pmatrix}, \quad (8)$$

where

$$\widetilde{h}_n = \begin{pmatrix} i\gamma & \nu & 0 & \kappa\tilde{J} \\ \nu & -i\gamma & \kappa\tilde{J} & 0 \\ 0 & \kappa\tilde{J} & 0 & \nu\tilde{Q} \\ \kappa\tilde{J} & 0 & \nu\tilde{Q} & 0 \end{pmatrix},$$

$$\widetilde{\sigma}_- = \begin{pmatrix} 0 & 0 & 0 & \kappa_1\tilde{J} \\ 0 & 0 & \kappa_1\tilde{J} & 0 \\ 0 & 0 & 0 & 0 \\ 0 & 0 & 0 & 0 \end{pmatrix}, \quad \widetilde{\sigma}_+ = \begin{pmatrix} 0 & 0 & 0 & 0 \\ 0 & 0 & 0 & 0 \\ 0 & \kappa_1\tilde{J} & 0 & 0 \\ \kappa_1\tilde{J} & 0 & 0 & 0 \end{pmatrix}.$$

Similarly, under PBC, by introducing the following transformation

$$c^{(1)}_q = \bar{c}^{(1)}_q,$$
$$c^{(2)}_q = \bar{c}^{(2)}_q,$$
$$c^{(3)}_q = \bar{c}^{(3)}_q e^{-i\frac{A}{\omega}\cos(\omega z)},$$
$$c^{(4)}_q = \bar{c}^{(4)}_q e^{i\frac{A}{\omega}\cos(\omega z)},$$

the correspondingly effective Hamiltonian in momentum space can be written as

$$H^{\text{eff}}(q) = \begin{bmatrix} i\gamma & \nu\,e^{iq} & 0 & \kappa_a\tilde{J} \\ \nu\,e^{-iq} & -i\gamma & \kappa_b^*\tilde{J} & 0 \\ 0 & \kappa_b\tilde{J} & 0 & \nu\,e^{iq}\tilde{Q} \\ \kappa_a^*\tilde{J} & 0 & \nu\,e^{-iq}\tilde{Q} & 0 \end{bmatrix}. \quad (9)$$

Here $\tilde{J} = J_0(A/\omega)$, $\tilde{Q} = J_0(2A/\omega)$, and $J_0(A/\omega)$ is the zero-order Bessel function. Therefore, the modulus of $\tilde{J}$ and $\tilde{Q}$ depend on the values of A/ω, and can change between zero and one. In particular, the modulus $|\tilde{J}|$ equals zero at some specific values of A/ω (such as $A/\omega \simeq 2.4$ and 5.52), and the modulus $|\tilde{Q}|$ equals zero at $A/\omega \simeq 1.2$ and 2.76. Diagonalizing the effective Hamiltonian (9), the quasienergies ε are given by

$$\varepsilon = \pm\sqrt{\frac{-X \pm \sqrt{X^2 - 4Y}}{2}}, \quad (10)$$

with

$$X = \gamma^2 - \nu^2(1 + \tilde{Q}^2) - 2\tilde{J}^2 D,$$
$$Y = -2\tilde{J}^2\nu^2\tilde{Q}D + (\nu^4 - \gamma^2\nu^2)\tilde{Q}^2 + \tilde{J}^4 D^2.$$

From Eq. (10), we can see for a fixed γ, κ, and κ_1, the spontaneous global $\mathcal{PT}$ symmetry breaking transition can be manipulated by tuning modulation parameter, because the modulus $|\tilde{J}|$ and $|\tilde{Q}|$ periodically change from zero to one with the modulation parameter A/ω.

For the special value $\tilde{J} = 0$, the quasienergies become $\varepsilon = \pm\tilde{Q}\nu$ and $\pm\sqrt{\nu^2 - \gamma^2}$. In this situation, the system decouples N uncoupled $\mathcal{PT}$ symmetric dimers, and hence the critical value of $\mathcal{PT}$ symmetry breaking transition is determined by single $\mathcal{PT}$ symmetric dimer. Therefore, the critical values of global $\mathcal{PT}$ symmetry breaking transition under OBC or PBC both are $\gamma_{\text{pbc}} = \gamma_{\text{obc}} = \nu = 1$. Similarly, for the special value $\tilde{Q} = 0$, the quasienergies become $\varepsilon = \pm\sqrt{\frac{2D\tilde{J}^2 + \Gamma \pm \sqrt{\Gamma(4D\tilde{J}^2 + \Gamma)}}{2}}$, where $\Gamma = \nu^2 - \gamma^2$. The critical values of global $\mathcal{PT}$ symmetry breaking transition under OBC and PBC are the same, $\gamma_{\text{pbc}} = \gamma_{\text{obc}} = \nu = 1$. Therefore, for the special values $\tilde{J} = 0$ or $\tilde{Q} = 0$, the critical values of global $\mathcal{PT}$ symmetry breaking transition are independent of parameters κ, κ_1, and the boundary condition. However, when $\tilde{J} \neq 0$ or $\tilde{Q} \neq 0$, the critical values γ_{pbc} and γ_{obc} can be manipulated by modulation parameter A/ω. That is mainly divided into the following two categories. (a) As A/ω increases from 0 to 1.2, the critical value γ_{pbc} can be adjusted from $\gamma_{\text{pbc}}^{(2)}$ to 1, but the critical value γ_{obc} cannot be tuned, and always is $\gamma_{\text{obc}} = \tilde{\gamma}_{\text{obc}} = 1$. (b) When $1.2 < A/\omega < 2.4$, the critical values γ_{pbc} and γ_{obc} can be simultaneously adjusted to less than 1. This implies that the domain of the BI-$\mathcal{PT}$ phase can be manipulated to be narrow and even disappears by tuned A/ω.

To verify the above analytical results, we show the phase diagram of global $\mathcal{PT}$ symmetry in the parameter plane (γ, κ_1) for different modulation parameters A/ω in Fig. 5. As an example, we choose the unmodulated case in Fig. 2(b) as a reference system. Obviously, the presence of periodic modulation modifies the previous physical picture. First, it
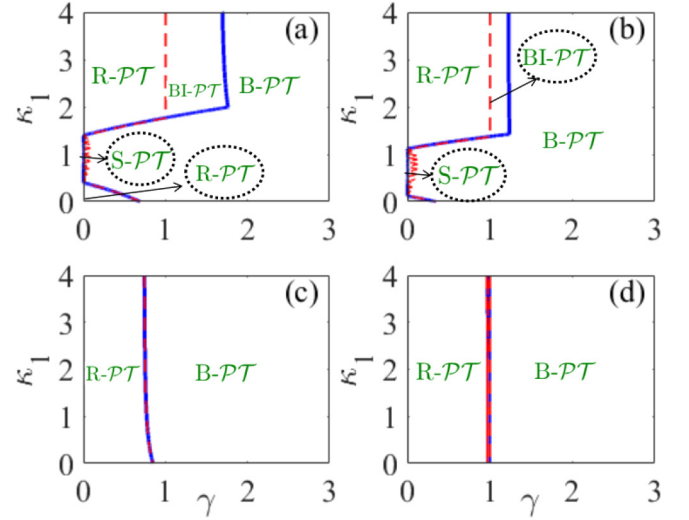

FIG. 5. Phase diagram of the system in the parameter plane (γ, κ_1) for different modulation parameters (a) $A/\omega = 0.6$, (b) $A/\omega = 1$, (c) $A/\omega = 1.5$, and (d) $A/\omega = 2.4$. Blue lines are numerical results obtained from the effective Hamiltonian (9) under PBC, and red lines are numerical results obtained from the effective Hamiltonian (8) under OBC. The other parameters are chosen as $N = 20$, $\kappa = 0.5$, $\omega = 10$, and $\nu = 1$.

clearly shows that the domain of the BI-$\mathcal{PT}$ phase can be manipulated to be narrow and even disappears by tuning A/ω, and hence the triple point also vanishes. Second, the domain of the B-$\mathcal{PT}$ phase under parameter region of $\gamma < 1$ can be an adjusted R-$\mathcal{PT}$ phase with the increase of A/ω. Then the phase space (γ, κ_1) only can be divided into two domains consisting of R-$\mathcal{PT}$ and B$\mathcal{PT}$ for $1.2 \leqslant A/\omega \leqslant 2.4$, where the critical values γ_{pbc} and γ_{obc} are independent of boundary condition, and can be simultaneously adjusted, as shown in Figs. 5(c) and 5(d). Especially, one can obtain a larger parameter region of unbroken global $\mathcal{PT}$ symmetry that is independent of boundary conditions by choosing zero points of $\tilde{J}$ or $\tilde{Q}$, such as Fig. 5(d). To see clearly how the spectra change in different phases with the increase of γ for different modulation parameters A/ω, we show the imaginary parts of the quasienergies as a function of γ for the system under OBC and PBC. Typical examples are displayed in Fig. 6 by choosing modulation parameters $A/\omega = 0.6$, 1.5, and 2.4. It clearly shows that the critical value $\tilde{\gamma}_{\text{obc}} \equiv 1$ is independent of modulation parameter A/ω, but the critical values γ_{obc} and γ_{pbc} can be adjusted by tuning A/ω. The critical value γ_{pbc} can change from $\gamma_{\text{pbc}}^{(2)}$ to 1 as A/ω increases from 0 to 1.2, and γ_{pbc} and γ_{obc} can be adjusted to be less than 1 for $1.2 < A/\omega < 2.4$. Therefore, when $\gamma_{\text{pbc}} \leqslant \tilde{\gamma}_{\text{obc}}$ for $1.2 \leqslant A/\omega \leqslant 2.4$, a pair of isolated zero-energy edge states embed into bulk states, and then the BI-$\mathcal{PT}$ phase disappears. This is why the BI-$\mathcal{PT}$ phase can be manipulated by tuning the modulation parameter in our system.

To show the parameter dependence of global $\mathcal{PT}$ symmetry from another angle, we show the quasienergies $|\text{Im}(\varepsilon)|$ as a function of A/ω and γ for different coupling parameters (κ, κ_1) both for PBC and OBC. As examples, we choose three sets of coupling parameters that initially are in the R-$\mathcal{PT}$
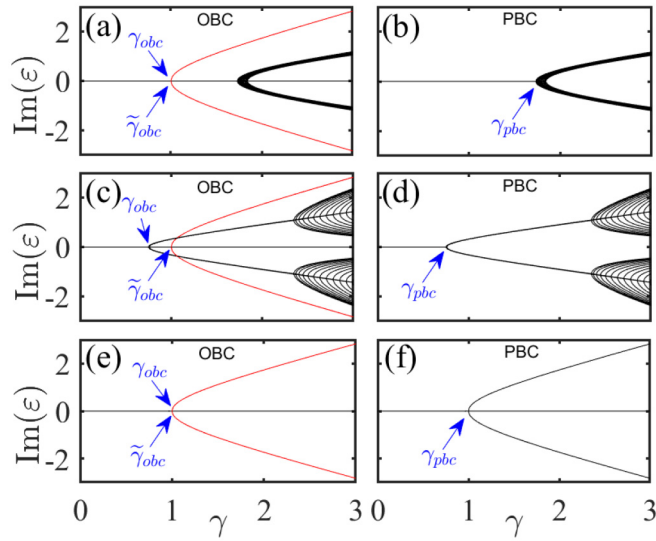
FIG. 6. Imaginary parts of the quasienergies of the system under OBC and PBC as a function of γ for $A/\omega = 0.6$ (top), 1.5 (middle), and 2.4 (bottom). The other parameters are $\omega = 10$, $\kappa_1 = 2.5$, $\kappa = 0.5$, $N = 20$, and $\nu = 1$.

phase ($\kappa = 0.5$, $\kappa_1 = 0.1$), B-$\mathcal{PT}$ phase ($\kappa = 0.5$, $\kappa_1 = 1$), and BI-$\mathcal{PT}$ phase ($\kappa = 0.5$, $\kappa_1 = 2$), as shown in Fig. 7. It is clear that, whether or not the system has initial global $\mathcal{PT}$ symmetry, the periodic modulation not only can restore the broken global $\mathcal{PT}$ symmetry, but also can control it by tuning modulation amplitude. Differently, the global $\mathcal{PT}$ symmetry only can be adjusted to the critical value $\gamma_{\text{obc}} = \nu = 1$ for parametric region that initially is in the R-$\mathcal{PT}$ phase, B-$\mathcal{PT}$ phase, and BI-$\mathcal{PT}$ phase of the system under OBC, whereas it can be adjusted to $\gamma_{\text{pbc}} > 1$ for the parametric region that initially is in the BI-$\mathcal{PT}$ phase of the system under PBC. Therefore, for our modulated system with fixed γ, it is possible to observe the spontaneous global $\mathcal{PT}$ symmetry-breaking
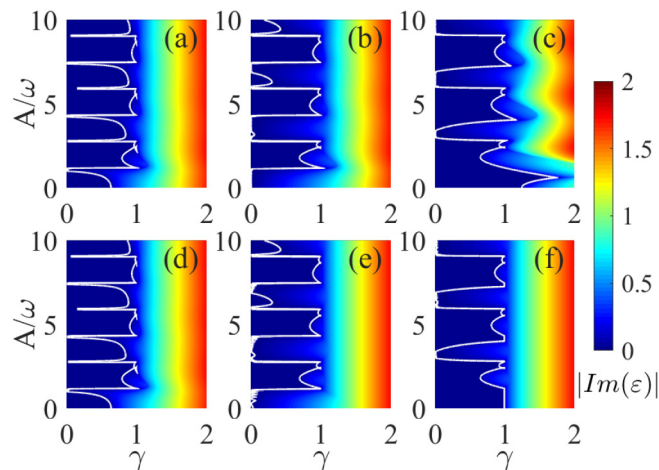

FIG. 7. Imaginary parts of the quasienergies $|\text{Im}(\varepsilon)|$ as a function of A/ω and γ under PBC (top) and OBC (bottom) with different coupling strengths $\kappa_1 = 0.1$ (left), $\kappa_1 = 1$ (middle), and $\kappa_1 = 2$ (right). The other parameters are chosen as $N = 20$, $\kappa = 0.5$, $\omega = 10$, and $\nu = 1$.
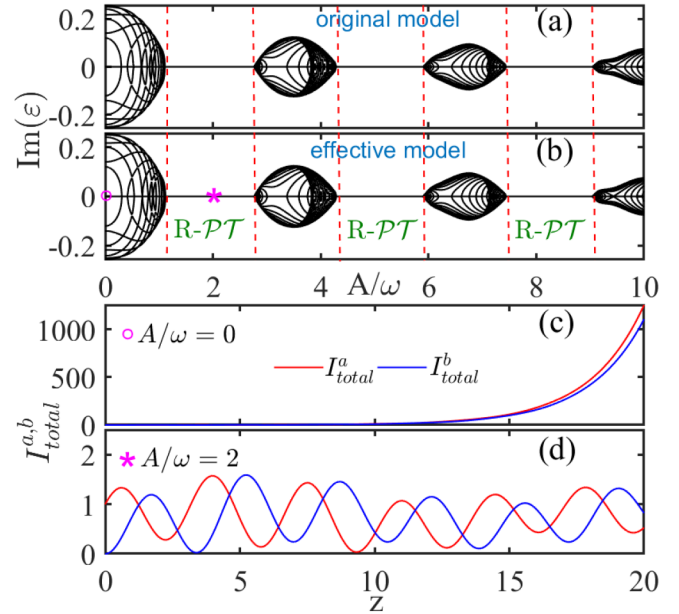

FIG. 8. Panels (a) and (b) show the imaginary parts of the quasienergies $\text{Im}(\varepsilon)$ as a function of A/ω from the original Hamiltonian (2) and effective Hamiltonian (8), respectively. Panels (c) and (d) show the total intensity $I_{\text{total}}^{a,b}$ evolution of the top and bottom row waveguides for (c) $A/\omega = 0$ and (d) $A/\omega = 2$. The other parameters are chosen as $N = 20$, $\kappa = 0.5$, $\kappa_1 = 1$, $\gamma = 0.5$, $\omega = 10$, and $\nu = 1$.

transition by tuning A/ω. Therefore, the global property of transverse periodic structure of such an array can be manipulated by only tuning modulation amplitude of longitudinal periodic modulation.

Finally, to show the validity of the high-frequency Floquet analysis, we compare the numerical results of the quasienergies ε obtained from the original Hamiltonian with the analytical ones obtained from the high-frequency Floquet analysis. We will show the ω dependence of $\text{Im}(\varepsilon)$. As an example, we show the imaginary parts of the quasienergies $\text{Im}(\varepsilon)$ as a function of A/ω from the original Hamiltonian (2) and effective Hamiltonian (8) in Figs. 8(a) and 8(b). It is important to note that, in our system, under the condition of $\omega/\kappa_1 \geqslant 10$ for a fixed $\kappa \leqslant \kappa_1$, the analytical results obtained from the effective Hamiltonian (8) via high-frequency Floquet analysis agree very well with the numerical results obtained from the original Hamiltonian (2). Especially, it is revealed that the periodic modulation can not only restore the broken global $\mathcal{PT}$ symmetry but also lead to periodical appearance of higher-order exceptional points by tuning modulation amplitude. In order to show that the initial broken global $\mathcal{PT}$ symmetry can be restored by using the periodic modulation, we show the intensity evolution given by Eq. (1) for the unmodulated and modulated cases in Figs. 8(c) and 8(d), where $I_{\text{total}}^a = \sum_n \sum_{j=1,4} I_{2n-s(j)}^a$ and $I_{\text{total}}^b = \sum_n \sum_{j=2,3} I_{2n-s(j)}^b$ are the total intensity of top and bottom row waveguides, respectively. For the unmodulated case, the total intensity $I_{\text{total}}^{a,b}$ shows unbounded growing, which is a direct signature of the broken global $\mathcal{PT}$ symmetry. For the modulated case with $A/\omega = 2$, the total intensity $I_{\text{total}}^{a,b}$ shows stationary periodic oscillations

along the propagation direction, which confirms the existence of global $\mathcal{PT}$ symmetry.

V. CONCLUSION AND DISCUSSION

In summary, we have investigated the static and dynamical property of global $\mathcal{PT}$ symmetry in an array of periodically modulated $\mathcal{PT}$ symmetric quadrimer waveguides. For the unmodulated case with inhomogeneous inter- and intraquadrimer coupling strength $\kappa_1 \neq \kappa$, in addition to conventional global $\mathcal{PT}$ symmetric phases and $\mathcal{PT}$ symmetry breaking phase, we find that there is an exotic phase where global $\mathcal{PT}$ symmetry is broken under OBC, whereas it still is $\mathcal{PT}$ symmetric under PBC. By comparing the energy spectra and dynamics in the different phases, it is revealed that there exists a pair of zero-energy edge states with purely imaginary energy eigenvalues localized at the left boundary in the BI-$\mathcal{PT}$ phase, whereas other $4N - 2$ eigenvalues are real. The parametric dependence of the spontaneous global $\mathcal{PT}$ symmetry breaking is analytically and numerically explored for the modulated array. Because critical value $\widetilde{\gamma}_{\mathrm{obc}}$ is independent of modulation parameter A/ω, and the critical value γ_{pbc} may decrease by tuning A/ω, the domain of the BI-$\mathcal{PT}$ phase can shrink and even disappear by tuning A/ω. More interestingly, whether or not the array has initial global $\mathcal{PT}$ symmetry, periodic modulation not only can restore the broken global $\mathcal{PT}$ symmetry, but also can control it by tuning the modulation amplitude. Therefore, the global property of transverse periodic structure of an optical array can be manipulated by only tuning the modulation amplitude of the longitudinal periodic modulation. Our results provide a promising approach for designing and manipulating optical material.

With currently available techniques, it is possible to realize our model and observe our theoretical predictions with experiments. Our proposed structure can be demonstrated experimentally in numerous optical systems [9,13,54,55]. For instance, in photonics, one can use the femtosecond direct writing method [56] to realize an array of $\mathcal{PT}$ symmetric photonic coupled waveguides. Periodic modulations can be introduced by harmonic modulations of the real refractive index or periodic curvatures along the propagation direction [57–59]. For such an optical array with periodic modulation, spontaneous global $\mathcal{PT}$ symmetry breaking transition may be observed by adjusting the modulation parameter. In addition, it is also possible to apply our model and method for designing some optical devices, such as single edge-mode laser and robust one-way edge mode transport.

[1] V. V. Konotop, J. Yang, and D. A. Zezyulin, Nonlinear waves in PT-symmetric systems, Rev. Mod. Phys. **88**, 035002 (2016).

[2] C. M. Bender, *PT Symmetry* (World Scientific, Singapore, 2019); D. Christodoulides and J. Yang, *Parity-Time Symmetry and Its Applications* (Springer, Berlin, 2018).

[3] N. Moiseyev, *Non-Hermitian Quantum Mechanics* (Cambridge University Press, Cambridge, UK, 2011).

[4] R. El-Ganainy, K. G. Makris, M. Khajavikhan, Z. H. Musslimani, S. Rotter, and D. N. Christodoulides, Non-Hermitian physics and PT symmetry, Nat. Phys. **14**, 11 (2018).

[5] C. M. Bender and S. Boettcher, Real Spectra In Non-Hermitian Hamiltonians Having PT Symmetry, Phys. Rev. Lett. **80**, 5243 (1998).

[6] C. M. Bender, Making sense of non-Hermitian Hamiltonians, Rep. Prog. Phys. **70**, 947 (2007).

[7] S. V. Suchkov, A. A. Sukhorukov, J. Huang, S. V. Dmitriev, C. Lee, and Y. S. Kivshar, Nonlinear switching and solitons in PT-symmetric photonic systems, Laser Photon. Rev. **10**, 177 (2016).

[8] C. V. Morfonios, P. A. Kalozoumis, F. K. Diakonos, and P. Schmelcher, Nonlocal discrete continuity and invariant currents in locally symmetric effective Schrödinger arrays, Ann. Phys. (NY) **385**, 623 (2017).

[9] S. Weimann, M. Kremer, Y. Plotnik, Y. Lumer, S. Nolte, K. G. Makris, M. Segev, M. C. Rechtsman, and A. Szameit, Topolog-

[10] M. Parto, S. Wittek, H. Hodaei, G. Harari, M. A. Bandres, J. Ren, M. C. Rechtsman, M. Segev, D. N. Christodoulides, and M. Khajavikhan, Edge-Mode Lasing in 1D Topological Active Arrays, Phys. Rev. Lett. **120**, 113901 (2018).

[11] N. X. A. Rivolta, H. Benisty, and B. Maes, Topological edge modes with PT symmetry in a quasiperiodic structure, Phys. Rev. A **96**, 023864 (2017).

[12] L. Ge, Y. D. Chong, and A. D. Stone, Conservation relations and anisotropic transmission resonances in one-dimensional PT-symmetric photonic heterostructures, Phys. Rev. A **85**, 023802 (2012).

[13] A. Regensburger, C. Bersch, M.-A. Miri, G. Onishchukov, D. N. Christodoulides, and U. Peschel, Parity-time synthetic photonic lattices, Nature (London) **488**, 167 (2012).

[14] Z. Gao, S. T. M. Fryslie, B. J. Thompson, P. S. Carney, and K. D. Choquette, Parity-time symmetry in coherently coupled vertical cavity laser arrays, Optica **4**, 323 (2017).

[15] D. J. Nodal Stevens, B. Jaramillo Ávila, and B. M. Rodríguez-Lara, Necklaces of PT-symmetric dimers, Photon. Res. **6**, A31 (2018).

[16] S. Longhi, Convective and absolute PT-symmetry breaking in tight-binding lattices, Phys. Rev. A **88**, 052102 (2013).

ically protected bound states in photonic parity-time-symmetric crystals, Nat. Mater. **16**, 433 (2017).

[17] C. M. Bender, M. Gianfreda, and S. P. Klevansky, Systems of coupled PT-symmetric oscillators, Phys. Rev. A **90**, 022114 (2014).

[18] D. A. Zezyulin and V. V. Konotop, Nonlinear Modes in Finite-Dimensional PT-Symmetric Systems, Phys. Rev. Lett. **108**, 213906 (2012).

[19] S. Longhi, PT phase control in circular multi-core fibers, Opt. Lett. **41**, 1897 (2016).

[20] S. V. Dmitriev, A. A. Sukhorukov, and Y. S. Kivshar, Binary parity-time-symmetric nonlinear lattices with balanced gain and loss, Opt. Lett. **35**, 2976 (2010).

[21] X. M. Yang, X. Z. Zhang, C. Li, and Z. Song, Dynamical signature of the moiré pattern in a non-Hermitian ladder, Phys. Rev. B **98**, 085306 (2018).

[22] H. Ramezani, T. Kottos, V. Kovanis, and D. N. Christodoulides, Exceptional-point dynamics in photonic honeycomb lattices with PT symmetry, Phys. Rev. A **85**, 013818 (2012).

[23] I. V. Barashenkov, L. Baker, and N. V. Alexeeva, PT-symmetry breaking in a necklace of coupled optical waveguides, Phys. Rev. A **87**, 033819 (2013).

[24] H. Ramezani, Non-Hermiticity-induced flat band, Phys. Rev. A **96**, 011802(R) (2017).

[25] P. A. Kalozoumis, C. V. Morfonios, F. K. Diakonos, and P. Schmelcher, PT-symmetry breaking in waveguides with competing loss-gain pairs, Phys. Rev. A **93**, 063831 (2016).

[26] V. V. Konotop, D. E. Pelinovsky, and D. A. Zezyulin, Discrete solitons in PT-symmetric lattices, Europhys. Lett. **100**, 56006 (2012).

[27] N. V. Alexeeva, I. V. Barashenkov, and Y. S. Kivshar, Solitons in PT-symmetric ladders of optical waveguides, New J. Phys. **19**, 113032 (2017).

[28] M. C. Zheng, D. N. Christodoulides, R. Fleischmann, and T. Kottos, PT optical lattices and universality in beam dynamics, Phys. Rev. A **82**, 010103(R) (2010).

[29] O. Bendix, R. Fleischmann, T. Kottos, and B. Shapiro, Optical structures with local PT-symmetry, J. Phys. A: Math. Theor. **43**, 265305 (2010).

[30] Y. N. Joglekar, D. Scott, and M. Babbey, Robust and fragile PT-symmetric phases in a tight-binding chain, Phys. Rev. A **82**, 030103(R) (2010).

[31] N. Bender, H. Li, F. M. Ellis, and T. Kottos, Wave-packet self-imaging and giant recombinations via stable Bloch-Zener oscillations in photonic lattices with local PT symmetry, Phys. Rev. A **92**, 041803(R) (2015).

[32] O. Bendix, R. Fleischmann, T. Kottos, and B. Shapiro, Exponentially Fragile PT Symmetry in Lattices with Localized Eigenmodes, Phys. Rev. Lett. **103**, 030402 (2009).

[33] B. P. Nguyen and K. Kim, Transport and localization of waves in ladder-shaped lattices with locally PT-symmetric potentials, Phys. Rev. A **94**, 062122 (2016).

[34] B. Zhu, R. Lü, and S. Chen, PT symmetry in the non-Hermitian Su-Schrieffer-Heeger model with complex boundary potentials, Phys. Rev. A **89**, 062102 (2014).

[35] M. Klett, H. Cartarius, D. Dast, J. Main, and G. Wunner, Relation between PT-symmetry breaking and topologically nontrivial phases in the Su-Schrieffer-Heeger and Kitaev models, Phys. Rev. A **95**, 053626 (2017).

[36] S. Lieu, Topological phases in the non-Hermitian Su-Schrieffer-Heeger model, Phys. Rev. B **97**, 045106 (2018).

[37] J. Hou, Y. J. Wu, and C. Zhang, Two-dimensional non-Hermitian topological phases induced by asymmetric hopping in a one-dimensional superlattice, arXiv:1906.03988v1.

[38] C. Yuce and Z. Oztas, PT symmetry protected non-Hermitian topological systems, Sci. Rep. **8**, 17416 (2018).

[39] L. Jin, Topological phases and edge states in a non-Hermitian trimerized optical lattice, Phys. Rev. A **96**, 032103 (2017); L. Jin and Z. Song, Bulk-boundary correspondence in a non-Hermitian system in one dimension with chiral inversion symmetry, Phys. Rev. B **99**, 081103(R) (2019).

[40] A. A. Sukhorukov, S. V. Dmitriev, S. V. Suchkov, and Y. S. Kivshar, Nonlocality in PT-symmetric waveguide arrays with gain and loss, Opt. Lett. **37**, 2148 (2012).

[41] S. Longhi, F. Cannata, and A. Ventura, Spontaneous PT symmetry breaking in Dirac-Kronig-Penney crystals, Phys. Rev. B **84**, 235131 (2011).

[42] N. Moiseyev, Crossing rule for a PT-symmetric two-level time-periodic system, Phys. Rev. A **83**, 052125 (2011).

[43] X. Lian, H. Zhong, Q. Xie, X. Zhou, Y. Wu, and W. Liao, PT-symmetry-breaking induced suppression of tunneling in a driven non-Hermitian two-level system, Eur. Phys. J. D **68**, 189 (2014).

[44] Y. N. Joglekar, R. Marathe, P. Durganandini, and R. K. Pathak, PT spectroscopy of the Rabi problem, Phys. Rev. A **90**, 040101(R) (2014).

[45] J. Gong and Q. H. Wang, Stabilizing non-Hermitian systems by periodic driving, Phys. Rev. A **91**, 042135 (2015).

[46] X. Luo, J. Huang, H. Zhong, X. Qin, Q. Xie, Y. S. Kivshar, and C. Lee, Pseudo-Parity-Time Symmetry in Optical Systems, Phys. Rev. Lett. **110**, 243902 (2013).

[47] Z. Zhou, B. Zhu, and L. Zhang, Analytical study on propagation dynamics of optical beam in parity-time symmetric optical couplers, Commun. Theor. Phys. **63**, 406 (2015).

[48] Y. Wu, B. Zhu, S. Hu, Z. Zhou, and H. Zhong, Floquet control of the gain and loss in a PT-symmetric optical coupler, Front. Phys. **12**, 121102 (2017).

[49] A. Y. Song, Y. Shi, Q. Lin, and S. Fan, Direction-dependent parity-time phase transition and nonreciprocal amplification with dynamic gain-loss modulation, Phys. Rev. A **99**, 013824 (2019).

[50] M. Chitsazi, H. Li, F. M. Ellis, and T. Kottos, Experimental Realization of Floquet PT-Symmetric Systems, Phys. Rev. Lett. **119**, 093901 (2017).

[51] G. P. Agrawal, *Application of Nonlinear Fiber Optics* (Academic Press, New York, 2008).

[52] H. Benisty, A. Lupu, and A. Degiron, Transverse periodic PT symmetry for modal demultiplexing in optical waveguides, Phys. Rev. A **91**, 053825 (2015).

[53] H. Wu and J. H. An, Floquet topological phases of non-Hermitian systems, Phys. Rev. B **102**, 041119(R) (2020).

[54] C. E. Rüter, K. G. Makris, R. El-Ganainy, D. N. Christodoulides, M. Segev, and D. Kip, Observation of parity-time symmetry in optics, Nat. Phys. **6**, 192 (2010).

[55] A. Guo, G. J. Salamo, D. Duchesne, R. Morandotti, M. Volatier-Ravat, V. Aimez, G. A. Siviloglou, and D. N. Christodoulides, Observation of PT-Symmetry Breaking in Complex Optical Potentials, Phys. Rev. Lett. **103**, 093902 (2009).

[56] A. Szameit and S. Nolte, Discrete optics in femtosecond-laser-written photonic structures, J. Phys. B: At. Mol. Opt. Phys. **43**, 163001 (2010).

[57] S. Longhi, Quantum-optical analogies using photonic structures, Laser Photon. Rev. **3**, 243 (2009).

[58] I. L. Garanovich, S. Longhi, A. A. Sukhorukov, and Y. S. Kivshar, Light propagation and localization in modulated photonic lattices and waveguides, Phys. Rep. **518**, 1 (2012).

[59] J. M. Zeuner, M. C. Rechtsman, Y. Plotnik, Y. Lumer, S. Nolte, M. S. Rudner, M. Segev, and A. Szameit, Observation of a Topological Transition in the Bulk of a Non-Hermitian System, Phys. Rev. Lett. **115**, 040402 (2015).